The numerical and experimental investigation of erosion induced leakage flow through guide vanes of Francis turbine

IOP Conf. Series: Earth and Environmental Science **240** (2019) 072002 doi:10.1088/1755-1315/240/7/072002

The numerical and experimental investigation of erosion induced leakage flow through guide vanes of Francis turbine

Sailesh Chitrakar[1], Hari Prasad Neopane[1], Ole Gunnar Dahlhaug[2]

[1]Department of Mechanical Engineering, Kathmandu University, Dhulikhel, Nepal
[2]Waterpower Laboratory, Department of Energy and Process Engineering, Norwegian University of Science and Technology, Trondheim, Norway
Email: sailesh@ku.edu.np

Abstract. In Guide Vanes (GV) of Francis turbines, a portion of the pressure head of water converts into velocity head. This causes high acceleration of the flow in GV before reaching the runner. Furthermore, GVs are accompanied with a small clearance gap at both ends to adjust the opening angle based on various operating conditions. In the case of sediment affected power plants, the hard fine particles mixed in water erode the connecting ends due to horse-shoe vortices. This erosion together with the head cover deflection due to water pressure increases the size of the gap. Due to the adjacent pressure and suction sides in GV, the flow passes through the gap from high pressure side to low pressure or suction side. This leakage flow disturbs the main flow in the suction side, which can be observed in the form of a vortex filament. Depending upon the GV profile and opening angle, the vortex can have different characteristics. This study uses numerical and experimental techniques to study the potential effects of the leakage flow in overall performances of the turbine. The experiment is done to measure the velocity field around GV using Particle Image Velocimetry (PIV) technique on a GV cascade rig. The GV in this rig corresponds to 1:1 scale model of 4.1 MW Francis turbine, with the chord length of 142 mm and span height of 97 mm. Similarly, 14 pressure sensors are placed around the GV cover plate to measure the GV loading. The velocity and pressure fields are compared with the results of CFD. In this study, two GV profiles (NACA0012 and NACA4412) and 7 opening angles (-5°, -3°, -1°, 0°, 1°, 3°, 5° compared to the design point) of the GV are studied. Results show that at Best Efficiency Point (BEP) and small opening or closing, the pressure difference between the adjacent sides of GV and consequently, the leakage flow and the intensity of the vortex filament in NACA4412 is less than in NACA0012. However, at high opening angle or during full load, the direction of the leakage flow in NACA4412 is in opposite direction due to small or negative GV loading compared to BEP. It is shown how these vortices affect the runner performances and how the particles erode the runner inlet as a consequence of these vortices.

1. Introduction

Erosion in hydraulic turbines due to sediment particles carried by water is one of the major challenges in the power plants of Indian sub-continent. The effect is predominant in both impulse [1] as well as reaction [2] type turbines. Depending upon the nature of the flow in turbines, different components erode with different mechanisms [3]. In the case of Francis turbines, the outlet of the runner erodes due to high relative velocity of water [4]. At the corners between facing plates and guide vanes (GV), horseshoe vortex [5] causes erosion, forming grooves of the guide vane profile [6]. It also erodes the end surfaces of the guide vane, increasing the size of the clearance gap. In a power plant of Nepal (Kaligandaki A, 48x3 MW), the size of the clearance gap is reported to have increased by a maximum of 2% of the total span height on each side [7]. The pressure difference between the two adjacent sides of the GV induces leakage flow through this gap, which aggravates the flow and causes more erosion in downstream runner blades [8].

A one GV cascade rig was built to study the characteristics of the leakage flow [9]. The rig is capable to produce similar flow field around one GV, compared to that in real turbine. A 3D model of the rig is shown in Figure 1. The velocity field around the GV was measured using PIV technique. It was concluded that the symmetric GV profiles are not suitable for sediment affected turbines because of bigger pressure difference and higher leakage flow through the gap [10]. CFD technique was implemented to compare the leakage flow in different NACA profiles having same maximum thickness in the same rig [11]. It was seen that asymmetric profiles having a flatter suction side is more suitable as GV profiles in sediment affected power plants. A comparative study was made between a symmetric (NACA0012) and two asymmetric (NACA2412 and NACA4412) in the rig using PIV technique [8]. It was observed that the flatter suction side reduces the pressure difference between two sides of the GV at designed condition. However, there were some limitations in the one GV rig, which included periodicity of the solution around adjacent GVs, lack of flexibility to test in off-designed conditions and different GV profiles. It was also studied in CFD that the cascade rig with three GVs would give better estimation of the flow field, compared to the real turbine [9].

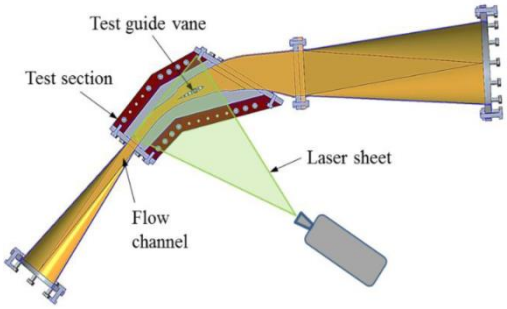

Figure 1. One GV cascade rig's test setup [10]

In this study, a three GV cascade rig was modelled and CFD was performed at 7 GV opening angles. At BEP, the results between the CFD and PIV of one GV cascade rig were compared with the three GV rig. The details about the CFD and PIV procedures in one GV rig is discussed in previous studies [8,11]. The major objective of this study is to compare the behaviour of leakage flow between NACA0012 and NACA4412 at various GV opening angles.

2. Literature study

The performance of NACA0012 and NACA4412 in airflows is found to have been studied in literatures [12,13]. These studies show that at 0^0 angle of attack, symmetric profiles have zero coefficient of lift, whereas asymmetric profiles contain some lift force at the same angle of attack. However, this is the case for a straight flow channel. In a recent study [8], it has been shown that when the symmetric profiles are oriented circumferentially forming a GV cascade, due to relative difference in the positions of the adjacent sides of the GV at a same chord length, a lift force exist even if the angle of attack is 0^0 with respect to the chord line.

In the case of airfoil containing clearance gaps, the term 'leakage flow' was defined in a study [14], as the flow occurring from the pressure side to the suction side, inside the gap between airfoil and end-walls. The same definition has been used in this study. Similarly, formation of the leakage vortex from leakage flow and its effect on the suction side flow has been discussed in a compressor cascade [15]. An investigation of tip clearance effects in turbine rotor concluded that the formation of the tip leakage vortex, its location and strength is related to the blade profile and pressure difference between the adjacent sides [16, 17]. Some numerical simulations were carried out in a turbine cascade, including a clearance gap with height of 1 percent span [18].

It is seen from literature that in the case of hydraulic turbines, limited works have been carried out in the field of leakage flow through blades. Some research works have been carried out in the clearance gap between the rotor and the stator of axial hydro turbines [19, 20]. These studies used PIV techniques to characterize the vortex core and its trajectory downstream of the hydrofoil. The study of the vortices in the case of GV of Francis turbine is a relatively new field, in which only few investigations have been carried out so far [8-11]. The effect of increasing clearance gap due to erosion by sand particles is a localized but serious problem. By using the knowledge and techniques to investigate such problems in other types of turbines, a methodology for this study was made.

3. Numerical model

Figure 1 shows the one GV cascade rig, where the CFD and PIV was carried out [8,10,11]. In this study, CFD was done in three GV cascade rig. The design principles of this rig are same as compared to the one GV rig [10]. The guide vanes were modelled with 2mm clearance gap on one end. The complete CFD domain is shown in Figure 2. The mass flow rate at inlet corresponds to four GV passages, which is equal to 391.67 kg/s. At outlet, pressure needed to avoid the negative pressure in the narrowest region of the rig was defined. The inlet diameter of the pipe is 400mm, whereas the chord length of each guide vane is 142.77mm.

Figure 2. CFD domain

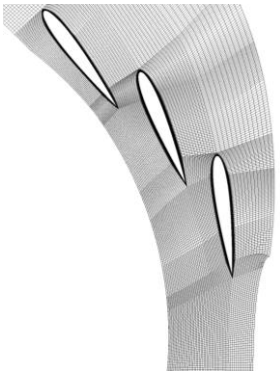

Figure 3. Mesh for CFD

The meshing was done using ICEM. O-grid was used at cylindrical inlet and outlet boundaries. Near the GV, the mesh was refined to resolve high gradients. The entire domain consisted of around 4.5 million hexahedral mesh elements. The clearance gap of 2mm consisted of 80 elements.
In this study, seven GV opening angles were compared. The designed case, or BEP is considered as 0^0 and other opening angles are with respect to this position. The GV closing are represented with negative values. In this case, simulations were performed for 1^0, 3^0, and 5^0 in both opening and closing GV positions. Separate domains were made for all the opening angles, but the mesh distribution was kept constant. All the simulations were performed with same boundary conditions.

3.1. Mesh Sensitivity

The estimation of the discretization error was done using GCI method [12] for 0^0 GV opening. In this method, the domain needs to be discretized with three different sizes of the mesh, with uniform increment. In this case, the grid refinement factor (r) was chosen to be 1.5X. Figure 4 shows the locations in the rig, where the parameters were measured. In the figure, the curve, SVo and GVo represent the circumferential position corresponding to stay vane outlet and guide vane outlet respectively.

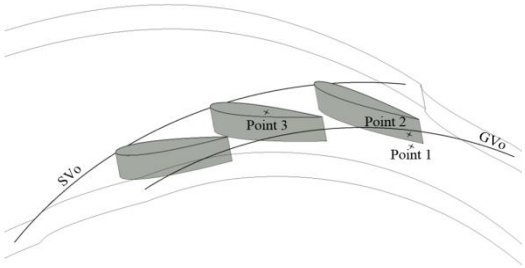

Figure 4. Locations of measurement for mesh sensitivity

Table 1 shows the significant parameters that were measured for the mesh sensitivity study. In the table, r_{21} is the exact value of the grid refinement factor between fine and medium mesh, whereas r_{32} is that between medium and coarse mesh. Φ represents the variable measured, which in this case is a component of the velocity. The subscript, 'ext' is the extrapolated value of the variable based on the three solutions. GCI is the numerical uncertainty values for different sizes of the mesh. In this case, Point 1 has the minimum uncertainty, because in this region, the unsteadiness in the flow is less, compared to Point 2 and Point 3.
Figure 5 shows average velocity in the GVo curve for different sizes of the mesh. The velocity deficit regions apart from the wall represent wake from each GV's trailing edges. The figure shows that the uncertainty in the result is high near wall regions. In other regions, the uncertainty was found to be within 2%.

Table 1. Results of mesh sensitivity study

	Parameter	Point 1	Point 2	Point 3
Velocity u (m/s)	r_{21}	1.55	1.55	1.55
	r_{32}	1.7	1.7	1.7
	$\Phi_{coarse(3)}$	5.82	-19.78	-14.6
	$\Phi_{medium(2)}$	5.73	-18.74	-16.16
	$\Phi_{fine(1)}$	5.77	-19.29	-17.4
	Φ_{ext}	5.84	-20.28	-19.65
	GCI^{21}_{fine}	0.0158	0.0648	0.1619
	GCI^{32}_{med}	0.0279	0.0987	0.1717

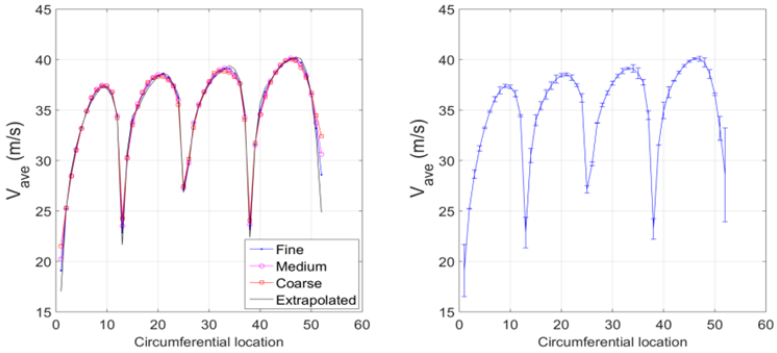

Figure 5. Average velocity along GVo curve

4. Results and discussions

The results are discussed in four sections. In the first part, the result of three GV cascade rig is compared with CFD and PIV done in one GV rig. It is to observe how closely the three results match with each other. In the second part, pressure along the GV stream (leading to trailing edge) is measured and compared between NACA0012 and NACA4412 at the midspan profile. The consequent vortices are then compared in terms of leakage flow factor and vortex travel. Finally, the torque at various chord-wise positions of the two profiles at all opening angles was compared.

4.1. Comparison between one and three GV rig

In this study, the comparison is done by taking the velocity contours at the mid-span plane for all the cases. Figure 6 shows the contour plot. The distribution of velocity in the test rig for all the cases are similar, especially around the leading edge, where the stagnation occurs, trailing edge profiles and pressure and suction side flows. The discussion about the comparison between CFD and PIV in one GV rig is presented in an earlier study [11]. In three GV rig, the contours are more periodic between adjacent GVs, which is closer to the real turbine. Due to the smaller cross section downstream of GVs in three GV rig, compared to the inlet mass flow rate, the maximum velocity in three GV is bigger than one GV rig.

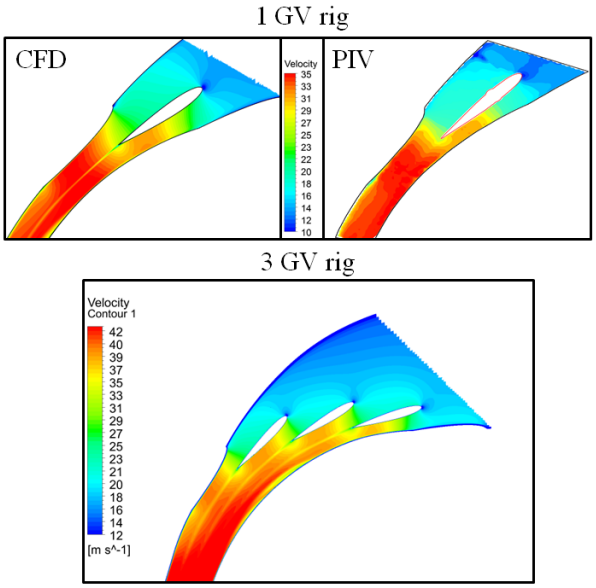

Figure 6. Velocity contours at midspan

4.2. GV loading

The area integral of the pressure difference between the two adjacent sides of a single GV gives a resultant force acting on the GV. The flow through the leakage gap depends on this resultant force. This GV loading was measured at midspan by measuring the pressure along the GV profile as shown in Figure 7. The measured pressure was normalized with the pressure at leading edge, which has been termed as Cp in the GV loading graph. This normalized pressure was plotted against the chord-wise position (x/c) from leading edge to trailing edge. In the plot, the red straight lines indicate the pressure in the pressure side whereas the black dotted lines indicate the pressure in the suction side. Figure 7 shows that at 0° opening angle with respect to BEP position, the GV loading in NACA0012 profile is higher than in NACA4412. It can also be seen from the graph that towards leading edge (x/c = 0.08), in NACA4412, the suction side pressure drops significantly. This could be because of an incorrect stagnation angle for NACA4412. It means that when a non-cambered profile is replaced with a cambered profile, the stagnation angle for BEP needs to be adjusted accordingly. In the present case, this drop in pressure could lead to some leakage flow at the leading edge for NACA4412 profile. However, it can be inferred that in overall, the leakage flow in NACA4412 is less than in NACA0012 for BEP.

Similarly, the GV loading for all the tested opening angles is shown in Figure 8. The negative degree with respect to BEP represents GV closing and positive degree represents GV opening. In hydropower plants, GV closing refers part load and GV opening refers full load operation. It can be seen from the figure that the GV opening reduces the GV loading. In the case of NACA0012, high opening angles makes the pressure difference minimum, which reduces the leakage flow through the clearance gap. The same effect also takes place in the case of NACA4412. However, at some point, the pressure difference becomes zero and at even higher opening angles, the pressure side experiences lower pressure than the original suction side. In such a condition, the leakage flow changes its direction. In the case of real turbines, the consequent vortices from the leakage flow do not enter the runner, but hit the adjacent GVs.

In the case of GV closing, the pressure difference increases for both the profiles. However, this difference is less in NACA4412 than in NACA0012. This infers that in part load conditions, the leakage flow in NACA4412 is less than in NACA0012.

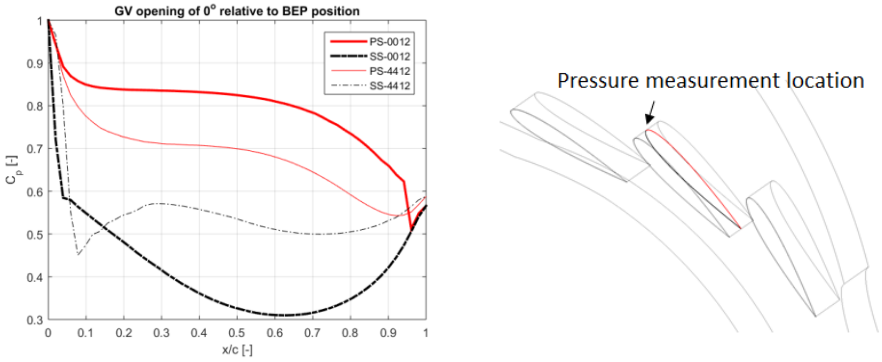

Figure 7. Pressure measurement at BEP

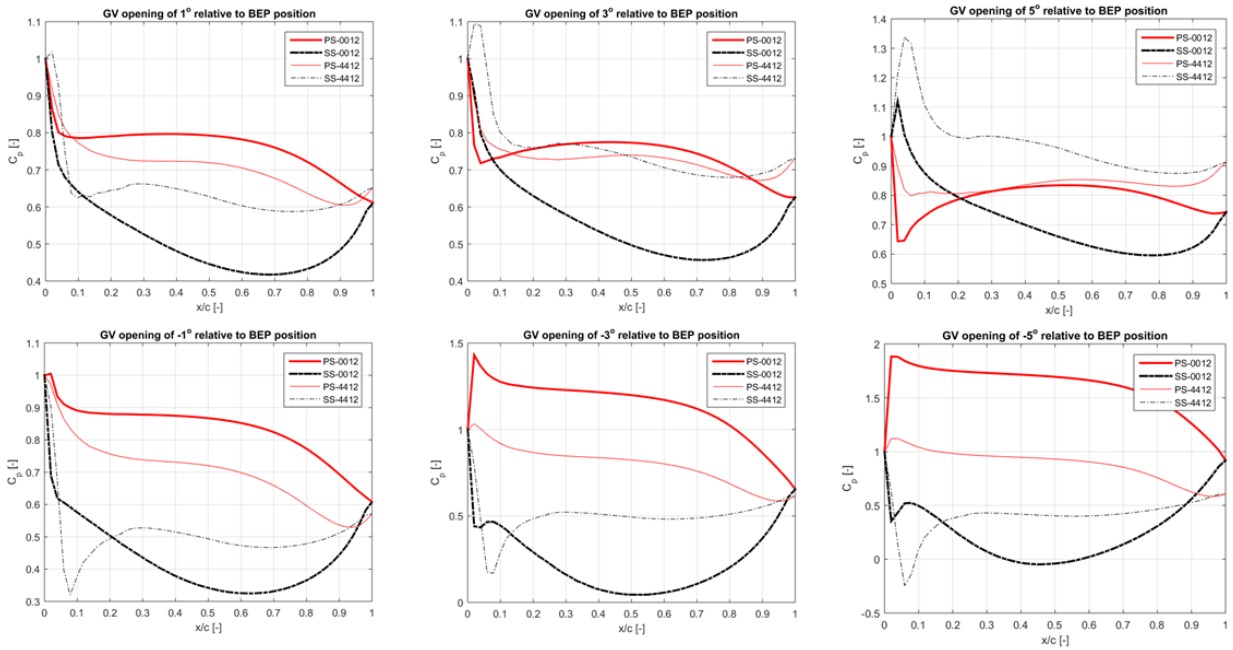

Figure 8. GV loading at different opening angles

4.3. Vortex filament

When a clearance gap is present at the ends of the GV, the pressure difference between the two sides induces leakage flow from high pressure to low pressure side. When this flow mixes with the main flow in the suction side, it results in the formation of a vortex, which is driven downstream additing to the total losses in case of turbines. The leakage flow in this study has been quantitatively compared between the two profiles by comparing Vy, which is the velocity component normal to the guide vane chord. In an ideal case, Vy component is zero, which means no leakage flow occurs inside the clearance gap.

Figure 9 compares the two profiles at BEP in terms of Vy. In the graph, the Vy component is plotted against the chordwise position of the GV. This figure shows that the Vy component is high after the mid-chord position. This trend is related to the GV loading curve shown in Figure 7. Compared to NACA0012, NACA4412 profile shows reduced Vy. The average value of Vy in NACA0012 for BEP is 27.4 m/s whereas in NACA4412, this value is 20.7 m/s. Figure 9 also shows the velocity vectors along the chord for the two profiles. It shows that the velocity gradient in the case of NACA0012 is high along the chord line. Figure 10 compares the Vy of the two profiles for $\pm 1^0$ and $\pm 3^0$. For GV closing, the average value of Vy for NACA0012 for -1^0 and -3^0 are 25.7 m/s and 24.1 m/s respectively, whereas these values are 20.7 m/s and 22.7 m/s respectively for NACA4412. It shows that the leakage flow in NACA4412 is less than in NACA0012 for all the GV closing angles. For GV opening, the average value of Vy for NACA0012 for 1^0 and 3^0 are 26.6 m/s and 18.62 m/s

respectively, whereas these values are 21.6 m/s and -11.2 m/s respectively for NACA4412. The graphs also show that the leakage flow for high GV opening angles is in the negative direction compared to the direction of Vy.

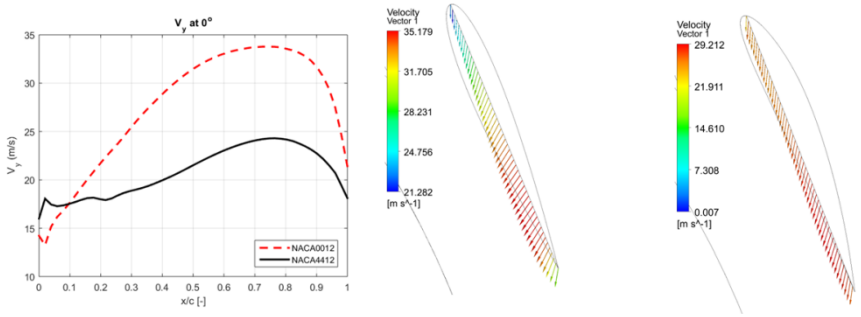

Figure 9. Vy component and velocity vectors along the chord line for NACA0012 and NACA4412

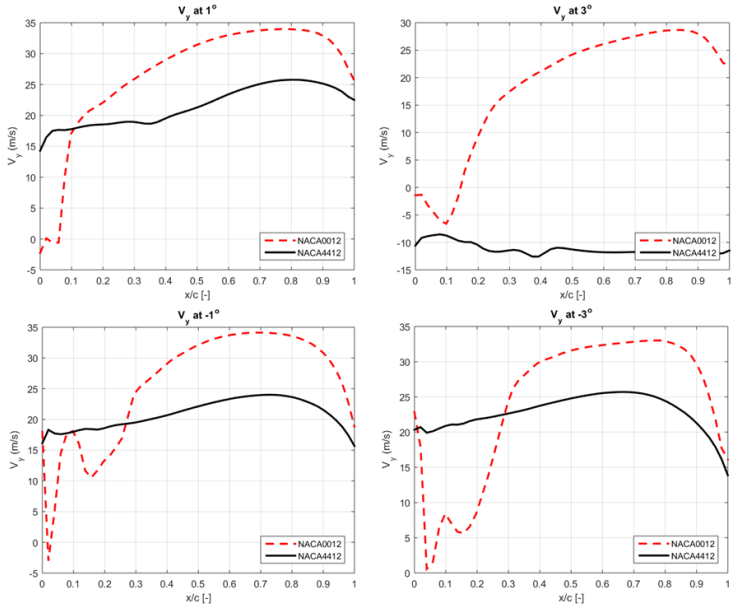

Figure 10. Vy component

The leakage flow leads to the formation of a vortex filament, which is shown in Figure 11-13. Five planes are defined perpendicular to the chord line of the middle GV, which are at a distance of 20 mm. In these planes, contours of total pressure normalized with the total pressure at the inlet are plotted. The value of this normalized pressure (CTP) is between 0 and 1, such that the values below 1 define losses. The vortex filaments are represented by low CTP values. By observing the adjacent planes, the path of these vortices can be traced. With the same contour value range, it can be seen from Figure 11 that the intensity of the vortex in NACA0012 is bigger than in NACA4412. In NACA4412, it can be seen that the vortex originates mostly from the leading edge. This justifies the GV loading curve shown in Figure 7, where the difference in pressure towards the leading edge for NACA0012 is high.
Figure 12 shows the CTP at -5^0 opening angle. Due to high pressure difference in the GV at closing conditions, the leakage flow and the consequent intensity of the leakage flow also increases. However, the intensity of the vortex in NACA4412 is smaller than in NACA0012. Figure 13 shows the CTP at 5^0 opening angle. In this case, it can be seen that the intensity of the vortex in NACA4412 is slightly bigger than in NACA0012. It can also be seen that the direction of this vortex in NACA4412 is in the opposite direction compared to other cases. Instead of entering the runner in the case of real turbine, such vortices will hit adjacent GVs and could cause more problems. Nevertheless, the distance between the adjacent GVs is larger than the distance between GVs and runner blades. Larger distance helps to dissipate the vortices and thus, minimize the effect.

From Sections 3.1, 3.2 and 3.3, it can be concluded that the cambered profiles reduces the pressure difference between the adjacent sides of the GV at the designed condition. In a straight flow channel, when the angle of stagnation is 0^0, the lift force in any symmetrical profile is zero. However, due to a circumferential orientation of the GV in turbines, a pressure difference is maintained between the adjacent sides at same chord length, even if the stagnation angle is 0^0 with respect to the chord line. Using asymmetrical profiles with flatter ends facing the runner, the difference in pressure can be reduced. This difference can be reduced for BEP and all GV closing angles. However, in GV opening angles, the difference in pressure gradually decreases for both the profiles. This decrease in GV loading affects NACA0012 positively, but in the case of NACA4412 at high opening angles, the pressure difference becomes negative. This changes the direction of the leakage flow and the consequent vortices.

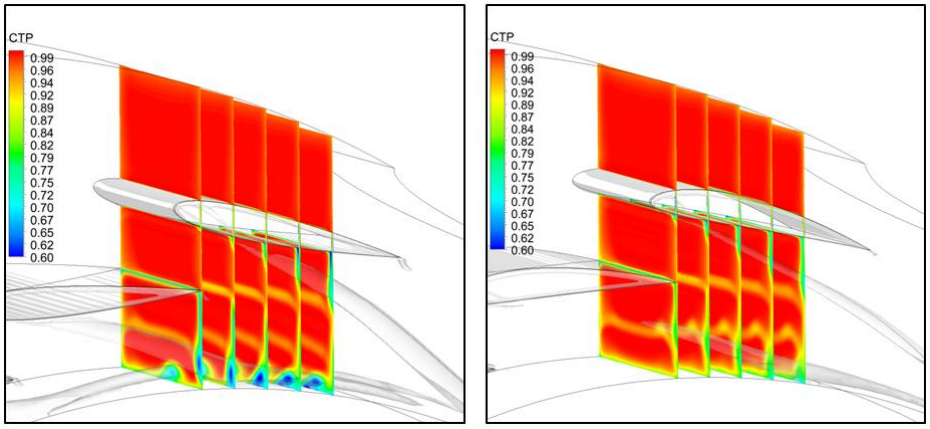

Figure 11. Total pressure contour at BEP, NACA0012 (left) and NACA4412 (right)

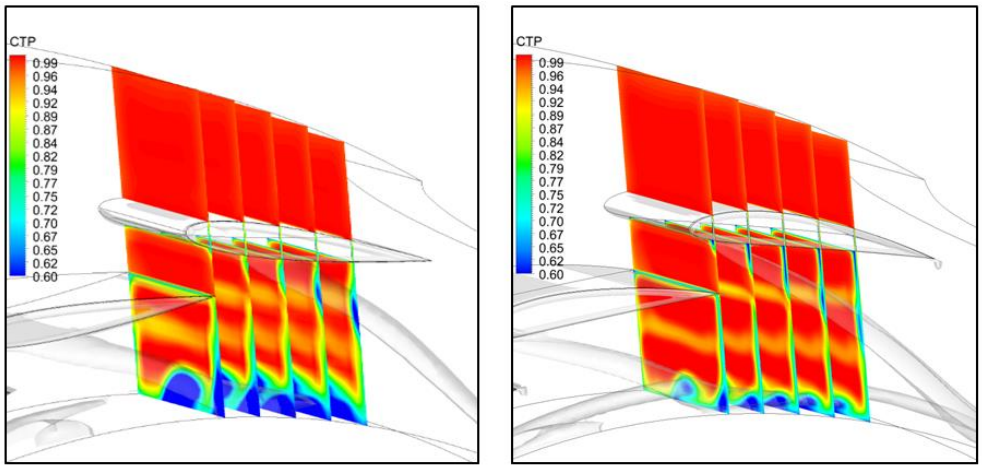

Figure 12. Total pressure contour at -5^0 with respect to BEP, NACA0012 (left) and NACA4412 (right)

4.4. Torque

When the GV rotates around the axis of the shaft, it induces torque in the GV due to the uneven pressure acting on it. It is desirable to have a minimum torque around the GV at all the operating conditions. The value of the torque depends on the position of the shaft. Figure 14 shows the values of the torque for all the opening angles, calculated with the shaft placed at locations from x/c = 0.35 to 0.52. It can be seen from the figure that the position of the shaft could be ideal for one operating condition, but it could result in a high torque in another condition. Hence an optimum position needs to be selected. In the case of NACA0012, when the shaft is placed at x/c = 0.41, a constant torque of around -50 N/m is constantly acting on the GV for all the opening angles.This contant torque can be reduced to around 15 N/m in the case of NACA4412, when the shaft is placed at x/c = 0.40.

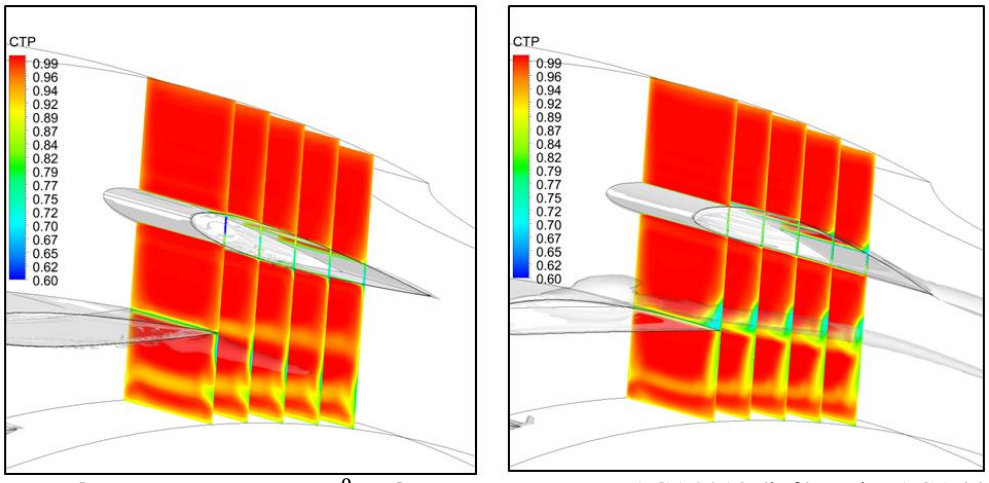

Figure 13. Total pressure contour at 5^0 with respect to BEP, NACA0012 (left) and NACA4412 (right)

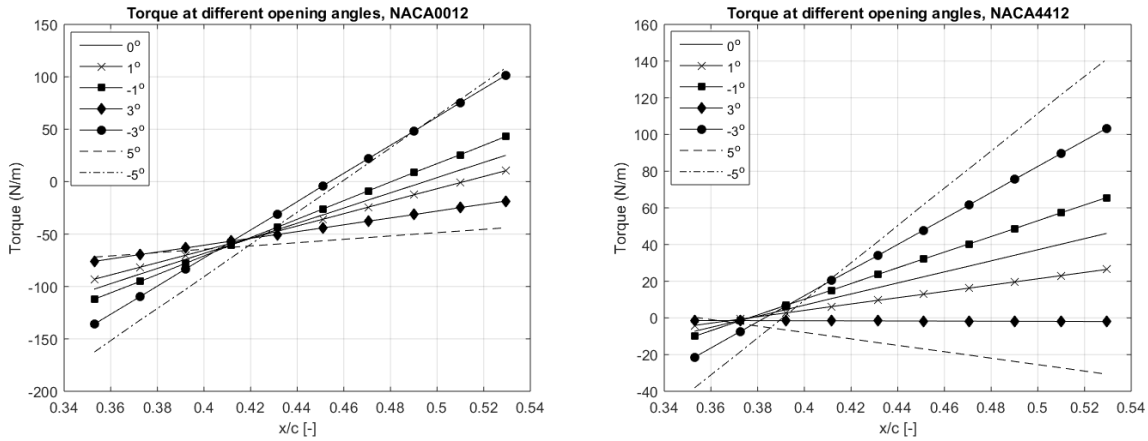

Figure 14. Torque acting on GV with two profiles

5. References

[1] Bajracharya T R, Acharya B, Joshi C B, Saini R P, and Dahlhaug O G 2008, Sand erosion of Pelton turbine nozzles and buckets: A case study of Chilime Hydropower Plant, Wear, vol. 264, pp. 177-184.

[2] Neopane H P, Thapa B, and Dahlhaug O G 2012, The Effect of Sediment Characteristics for Predicting Erosion on Francis Turbines Blades, The International Journal on Hydropower & Dams, vol. 19, no. 1, pp. 79-83.

[3] Chitrakar S, Neopane H P, and Dahlhaug O G 2016, Study of the Simultaneous Effects of Secondary Flow and Sediment Erosion in Francis Turbines, Renewable energy, vol. 97, pp. 881-891.

[4] Thapa B S, Thapa B, and Dahlhaug O G 2012, Empirical modelling of sediment erosion in Francis turbines, Energy, vol. 4, no. 1, pp. 386-291.

[5] Baker C J 1991, The Oscillation of Horseshoe Vortex Systems, J. Fluids Eng., 113, pp. 489-495.

[6] Brekke H, Wu Y, and Cai B Y 2002, Design of Hydraulic Machinery Working in Sand Laden Water, in Abrasive Erosion and Corrosion of Hydraulic Machinery, Imperial College Press, pp. 155-233.

[7] Koirala R, Thapa B, Neopane H P, Zhu B, and Chhetry B 2016, Sediment Erosion in Guide Vanes of Francis Turbine: A Case Study of Kaligandaki Hydropower Plant, Nepal, Wear, vol. 362-363, pp. 53-60.

[8] Chitrakar S, Neopane H P, Dahlhaug O G 2017, PIV investigation of the leakage flow through clearance gaps in cambered hydrofoils, J. Fluids Eng. Vol. 139, p. 091201.
[9] Thapa B S, Trivedi C, and Dahlhaug O G 2016, Design and Development of Guide Vane Cascade for a Low Speed Number Francis Turbine, Journal of Hydrodynamics, Ser. B, Vol. 28, Issue 4, pp. 676-68.
[10] Thapa B S, Dahlhaug O G and Thapa B 2017, Sediment Erosion Induced Leakage Flow from Guide Vane Clearance Gap in a Low Specific Speed Francis Turbine, Renewable Energy, 107, pp. 253-261.
[11] Chitrakar S, Thapa B S, Dahlhaug O G , Neopane H P 2017, Numerical and experimental study of the leakage flow in guide vanes with different hydrofoils, Journal of Computational Design and Engineering, vol. 4(3), pp. 218-230.
[12] Johnson J P, Iaccarino G, Chen K H and Khalighi B 2014, Simulations of High Reynolds Number Air Flow Over the NACA-0012 Airfoil Using the Immersed Boundary Method, ASME J. Fluids Eng., vol. 136(4), 040901.
[13] Maddah S R, Brunn H H 2001, An Investigation of Flow Fields Over Multi-Element Aerofoils, ASME J. Fluids Eng., vol. 124 (1), pp. 154-165.
[14] Heyes F J G, Hodson H P and Dailey G M 1992, The Effect of Blade Tip Geometry on the Tip Leakage Flow in Axial Turbine Cascades, Journal of Turbomachinery, vol. 114, 643-651.
[15] Jingjun Z, Shaobing H, Huawei L and Xiaoxu K 2012, Effect of Tip Geometry and Tip Clearance on Aerodynamic Performance of a Linear Compressor Cascade, Chinese Journal of Aeronautics, vol. 23(3), pp. 583-593.
[16] Yaras M I and Sjolander S A, 1992 Effect of Simulated Rotation on Tip Leakage in a Planar Cascade of Turbine Blades: Part I – Tip Gap Flow, Journal of Turbomachinery, vol. 114, pp. 652-659.
[17] Yaras M I, Sjolander, S A and Kind R J 1992, Effect of Simulated Rotation on Tip Leakage in a Planar Cascade of Turbine Blades: Part II – Downstream Flow Field and Blade Loading, Journal of Turbomachinery, vol. 114, pp. 660-667.
[18] Tallman J and Lakshminarayana B 2001, Numerical simulation of tip leakage flows in axial flow turbines, with emphasis on flow physics: Part I - Effect of tip clearance height, Journal of Turbomachinery, vol. 123, pp. 314-323.
[19] Aeschlimann V, Beaulieu S, Houde S, Ciocan G D, and Deschenes C 2013, Inter-blade Flow Analysis of a Propeller Turbine Runner Using Stereoscopic PIV, European Journal of Mechanics B/Fluids, vol. 42, pp. 121-128.
[20] Dreyer M, Decaix J, Munch-Alligne C, and Farhat M 2014, Mind the gap: a new insight into the tip leakage vortex using stereo-PIV, Exp Fluids, vol. 55, no. 11.
[21] Celik I B, Ghia U, Roache P, Freitas C, Coleman H, and Raad P 2008, Procedure for Estimation and Reporting of Uncertainty due to Discretization in CFD Applications, ASME J. Fluids Eng., vol. 130, pp. 078001

Acknowledgments
This study was carried out as a part of a joint PhD study between Kathmandu University (KU) and Norwegian University of Science and Technology (NTNU).